BioProcess International eBooks

BIOREACTOR DESIGN

LEVERAGING ESTABLISHED PRINCIPLES AND MODERN INSIGHTS

NaveenGanesh Muralidharan, Tyler Younger, Grace Chan, Shandilyn Ball, Mark Davis, and Emma Bolduc; Ken Clapp

March 2025

Bioreactor Design

Leveraging Established Principles and Modern Insights

NaveenGanesh Muralidharan, Tyler Younger, Grace Chan, Shandilyn Ball, Mark Davis, and Emma Bolduc; Ken Clapp

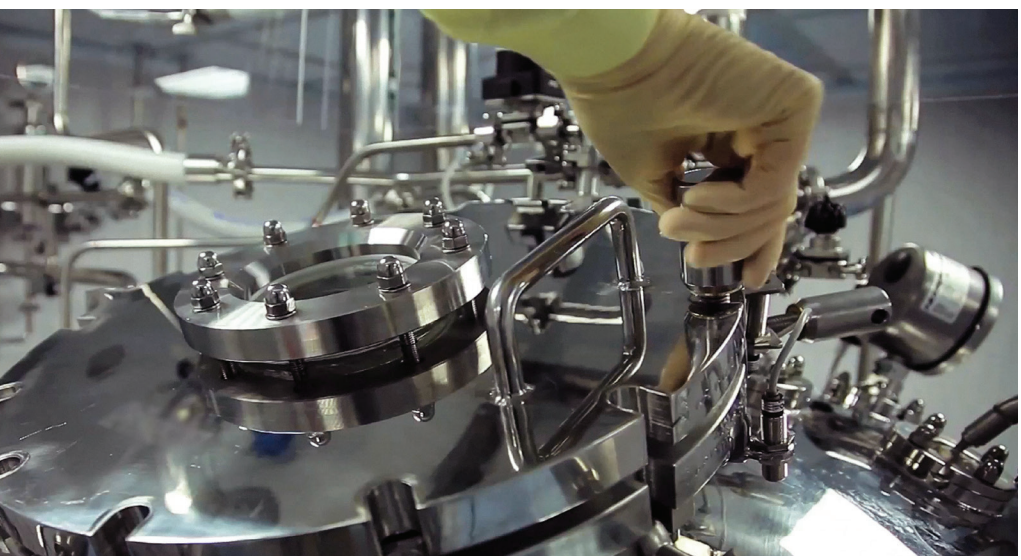

As demand grows for cultures with increasingly higher cell densities, bioreactor engineers and users are finding it necessary to understand the demands of current reactor designs and to conceive of new possibilities. Herein, writers from AGC Biologics explore key literature on bioreactor design, highlighting primary principles and common design choices. Then, a senior scientist from eBook sponsor Cytiva describes his team's concurrent development of computational fluid dynamics (CFD) models and the new Xcellerex X-platform bioreactor.

"The question isn't, '**Will** I need to scale up?' but, '**When** do I scale out or intensify?'"

Niklas Jungnelius
Bioprocess Modeling Leader, Cytiva

Knowing you need to get more out of your bioprocess is one thing. Deciding how to do it is another.

In our eBook, 14 Cytiva experts answer key questions on process intensification and scale-up – so you can choose the right path forward with confidence.

Download now ▶

cytiva.com

For local office contact information, visit cytiva.com/contact

CY50010-27Feb25-AD

Large-Scale Stirred-Tank Bioreactors

Key Design Parameters and Considerations for Cell-Culture Operations

NaveenGanesh Muralidharan, Tyler Younger, Grace Chan, Shandilyn Ball, Mark Davis, and Emma Bolduc

Cell-culture operating conditions often are limited by a bioreactor's design. Over the past few decades, as demand has grown for culture processes with increasingly higher cell densities, bioreactor suppliers have continued working to understand the demands and weaknesses of current bioreactor designs. Herein, we review design considerations for stirred-tank bioreactors (STRs) used in mammalian cell culture, including bioreactor aspect ratio, impeller type and number, and drilled-sparger configuration. We assess such factors' influences on shear stress and mixing time, which are essential to achieving desired cell-culture conditions and productivity. We also address common challenges (e.g., impeller flooding) and emphasize the importance of enhancing gas–liquid interactions to maintain suitable environments for cell growth. Special attention is given to the design of drilled-hole spargers, highlighting their effects on shear forces, bubble dynamics, and bubble-bursting behavior at liquid surfaces. Our review also provides information about the design and sizing of vent filters and mass-flow controllers (MFCs) as well as practical recommendations for improving bioreactor performance and efficiency. By integrating such insights into a handy resource, we aim to contribute to further advancements in bioreactor design and operation, enhancing biopharmaceutical production.

Figure 1: "Rule-of-thumb" parameters for stirred-tank reactor design

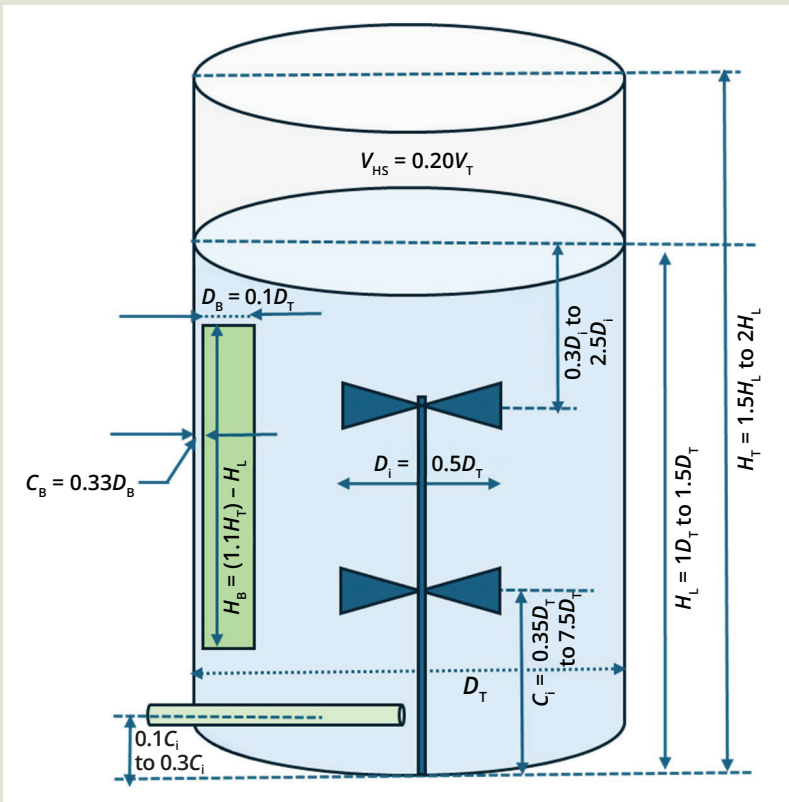

C_B = baffle clearance from tank bottom, C_i = impeller clearance from tank bottom, D_i = impeller diameter, D_T = tank diameter, H_B = baffle height, H_L = liquid height in tank, H_T = tank height, V_{HS} = headspace volume, V_T = total tank volume

Back to Contents

Building Blocks for Bioreactor Design

In large-scale STRs, optimizing performance requires careful consideration of design parameters such as vessel aspect ratio, headspace, and impeller configuration. Values for *bioreactor aspect ratio* — the proportion of culture liquid height (H_L) to tank diameter (D_T) — typically range from 1.0 to 1.5 (Figure 1, see previous page). Headspace is kept at 20% of the total geometric reactor volume to facilitate gas exchange and accommodate foam. The recommended ratio of total vessel height (H_T) to tank diameter is 1.5–2.0 (**1**).

Baffle Design: Baffles play a critical role in enhancing mixing efficiency and improving overall process performance. The number, location, and width of baffles are key design parameters that significantly affect fluid dynamics and mass transfer within a reactor. Ideally, a bioreactor should have four baffles, although three baffles can provide adequate mixing. Using more than four baffles does not improve mixing efficiency significantly (**2**). The width of each baffle (W_B) is typically 0.08× to 0.1× that of the tank diameter (D_T), ensuring that a baffle is sufficiently wide to disrupt solution flow and promote effective turbulence without causing excessive resistance (**1**). The recommended clearance for baffles (C_B) from a vessel tank is represented as either $C_B = 0.01 \times D_T$ or $C_B = 0.33 \times W_B$, with the recommended baffle height (H_B) equaling $(1.1 \times H_T) - H_L$ (**1, 3**).

Choice of Impeller: When selecting impellers for cell-culture bioreactors, careful consideration of shear sensitivity and mixing efficiency is crucial for optimizing performance. For mammalian cell cultures, which are highly sensitive to shear forces, pitched blade turbines and marine propellers typically are preferred for their low-shear characteristics, which help to minimize cell damage while ensuring effective mixing (**4, 5**). High-shear impellers, such as Rushton turbines, generally are inappropriate in these applications as they can induce significant shear stress that may harm delicate cells (**4, 5**).

The ratio of impeller diameter to tank diameter (d_i/D_T) typically ranges from 0.35 to 0.55, with a preferred value of 0.5 for bioreactor operation. The choice of impeller is determined by a cell line's sensitivity and specific mixing requirements (**1, 3**).

Impeller Numbers and Spacing: A general guideline is to use between one and three impellers in a cell-culture bioreactor, depending on the reactor volume and impeller type. Low-shear impellers may be best for shear-sensitive processes, and the number of impellers can be adjusted accordingly. To achieve suitable power input, scientists should arrange for the distance between impellers to be 1.2× to 1.5× the impeller diameter. Such spacing ensures that impellers will operate independently from one other (**6**).

Positioning of Bottom Impellers: In STRs, liquid height must be maintained above that of an impeller at a value 0.3× to 2.5× greater than the impeller diameter. Keeping the liquid level at 0.3× that of the d_i minimizes the risk of excessive foaming,

whereas a maximum height of 2.5× the d_i value prevents poor mixing. For best results, a volume of 0.5× to 1.0× the d_i value is recommended for operation. Moreover, the impeller clearance from the bottom of the tank should be set between 0.35× and 0.75× the D_T value to ensure efficient mixing and prevent dead zones (**3**).

Mixing-Time Requirements

Several factors influence bioreactor mixing time (t_{mix}), including impeller design, reactor geometry, and operating conditions (**7**). Optimizing mixing time is critical for efficient cell-culture operations. Effective mixing ensures uniform distribution of nutrients, oxygen, and cells, helping to maintain culture viability and productivity. Optimal t_{mix} values also are critical for achieving target cell densities and preventing formation of nutrient gradients, which can impede cell growth and diminish culture productivity (**8**). Reducing t_{mix} while ensuring uniform conditions can improve culture performance and control over cell metabolism (**9**).

Bioreactor mixing time refers to the duration required for culture solution to reach a specified level of homogeneity starting from a completely segregated state. Homogeneity is achieved after multiple circulations of reactor contents. According to Doran, for an STR equipped with several baffles and a low d_i/D_T ratio, the t_{mix} value is about 4× the circulation time (t_{cir}) needed for 95% homogeneity (Equation 1) (**7**). *Circulation time* represents how long it takes for an entire bioreactor volume to pass through an impeller. Mathematically, it is the ratio of liquid volume (V_L, in m^3) to impeller discharge rate (Q_{imp}, in m^3) (**7**). The *impeller discharge rate* represents the volume of fluid moved by an impeller per unit of time, as shown in Equation 1 (**7**), in which N_F is the impeller flow number and N is the impeller agitation rate in revolutions per minute (rpm):

Equation 1: $$4 \times t_{cir} = 4V_L \div Q_{imp} = 4V_L \div (N_F \times N \times d_i^3)$$

Understanding N_F values for different impellers ensures effective agitation and thereby improves process efficiency. Expressing a ratio between t_{mix} and N, an *impeller flow number* provides a dimensionless measure of an impeller's mixing performance. Reported values for different impeller types offer valuable insights into their relative efficiencies and operational characteristics.

Designed for gentle mixing, marine impellers have low N_F values, generally around 0.5. Pitched-blade impellers, including A310, A315, and A320 variants, exhibit a range of flow numbers that reflect their respective mixing efficiencies. A310 impellers typically have an N_F value of 0.3, providing a balance between mixing performance and shear force, whereas N_F values for A315 impellers generally are around 0.75, indicating slightly higher efficiency and moderate shear levels. A320 impellers are known for optimal mixing performance, and they usually feature N_F values of 0.62, making them particularly effective for applications requiring efficient yet gentle agitation (**4**).

Back to Contents

Reported N_F values are instrumental in guiding selection of impellers for specific applications. By considering such features, process engineers and scientists can make informed decisions to optimize mixing conditions and achieve desired outcomes.

Figure 2: Oxygen characteristic time (t_C) against viable-cell density (VCD)

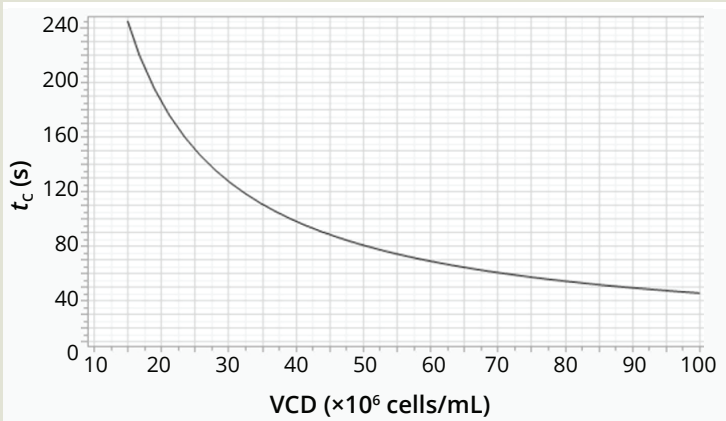

Oxygen Requirements:
Bioreactor mixing time significantly affects dissolved oxygen (DO) gradients, which are essential for optimizing culture conditions. The *oxygen characteristic time* (t_C) is a ratio of the oxygen concentration (C^*) in a feeding gas to the rate of cellular oxygen consumption, expressed as shown below (**9**):

Equation 2: $t_C = C^* \div OUR$

Muralidharan et al. have demonstrated that, under typical bioreactor operating conditions at 37 °C and 1 atm pressure, the oxygen uptake rate (OUR) can be determined by this equation (**9**):

Equation 3: $OUR = X_i \times SCR = 0.23 \times X_i (mmol/L{\cdot}h)$

That calculation is the product of a culture's viable cell density (X_i, in units of 10^6 cells/mL culture) and cells' specific oxygen-consumption rate, with Q_{02} estimated at 5.5 pmol/cell·day (**9, 10**).

Using Equation 2, process engineers can plot t_C values against viable cell densities (VCDs). Figure 2 provides such a plot, indicating that for a cell density of 50 million cells/mL, a t_{mix} value of <60 seconds is necessary to prevent heterogeneity and maintain uniform oxygen distribution within a bioreactor.

Shear from Impeller Agitation

In STRs, shear forces generated by impeller agitation significantly influence cell viability and productivity. Impeller-tip speed (U_{tip}) is a key parameter here because it directly influences localized shear rates and consequently the shear stress that cells experience (**11**). Values for U_{tip} (in m/s) can be calculated as shown here:

Equation 4: $U_{tip} = (\pi \times D_i \times N) \div 60$

Tip speeds should be <1.8 m/s to protect cells from excessive shear stress, which can hinder their growth and functionality (**9**).

Design of Drilled-Hole Spargers

Mammalian cells are particularly sensitive to the high shear forces generated by microspargers, which can diminish cell viability and

Back to Contents

productivity. Consequently, we concentrate on the design and optimization of drilled-hole spargers as an alternative. By providing gentle, controlled gas dispersion, such spargers mitigate some shear stress in a culture environment, thereby improving process outcomes. Our focus is supported by recent studies indicating that drilled-hole spargers offer more-uniform and less-disruptive gas transfer than that from microspargers. Below we describe a general method for designing drilled-hole spargers.

Find the Oxygen Demand and Required $k_L a$ for a Bioreactor Design: OUR is a pivotal parameter in bioreactor design, quantifying the rate at which cells consume oxygen during culture. Representing the amount of oxygen depleted per unit volume per unit time, OUR values for mammalian-cell cultures often are expressed in units such as mg/L·h or mmol/L·day (**1**). The parameter serves as a direct measure of culture metabolic activity, reflecting both the biological demand for oxygen and the efficiency of oxygen-transfer systems within a bioreactor. By evaluating OUR, process engineers can determine a culture's oxygen demand, then design appropriate aeration and agitation systems to meet those requirements (**1**). Such assessment ensures that a bioreactor will provide sufficient oxygen to sustain cell growth and productivity, thereby optimizing process performance and supporting scale-up strategies. Accurate OUR measurements help in adjusting operational parameters to maintain optimal culture conditions and achieve desired outcomes in both research-scale and industrial bioprocesses.

OUR values can be calculated from SCRs using a straightforward formula that incorporates cell density (see Equation 3). That relationship directly translates the metabolic activity of individual cells into a bulk measure of oxygen consumption for an entire culture. By multiplying an SCR value by the cell density, the OUR quantifies the total oxygen consumption rate per unit volume of a culture medium, providing essential information for oxygen transfer rate (OTR) requirements in a given bioreactor (**7**). Accurate calculation of OUR is crucial for maintaining appropriate oxygen levels and optimizing cell growth and productivity.

Muralidharan et al. have reviewed SCRs across different cell lines and bioreactor culture conditions (**10**). That study also examined typical cell densities observed in biomanufacturing processes. Based on their investigation, the writers recommended an SCR value of 5.5 pmol/cell·day as a reliable estimate for designing bioreactors. The review also demonstrated that for every 1 million cells/mL, the OUR is 0.23 mmol/L·h (**10**). Therefore, if a bioreactor is designed to support 50 × 10^6 cells/mL, then the required OUR value should be greater than 50 × 0.23 mmol/L·h = 11.5 mmol/L·h. Typically, bioreactors are designed to support 30 mmol/L·h (**1**). Assuming a sparging regimen with pure oxygen, Muralidharan et al. showed that a volumetric oxygen mass-transfer coefficient ($k_L a$) of 1 (1/h) can support about 4 × 10^6 cells/mL (**10**). Therefore, if a bioreactor is designed to support 50 × 10^6 cells/mL, then the required $k_L a$ value should be greater than (50 ÷ 4) = 12 (1/h).

Find the Required Gas Flow Rate (Q_g) from the k_La Value: The simplest and most practical approach to designing bioreactor spargers, particularly when process-specific information is unavailable, involves a "rule-of-thumb" setting, with the total gas flow rate for sparging at 0.05 volumes of gas per volume of liquid per minute (vvm). That guideline provides a reliable starting point for ensuring adequate gas transfer and distribution in the absence of detailed process data (**12, 13**).

When process information is available, process engineers can determine gas-flow rates based on k_La values to ensure that bioreactor designs will meet process-specific oxygen demands. Estimating k_La values is critical to optimizing the efficiency of gas–liquid mass transfer (**14**). The van 't Riet model is a widely used empirical correlation for k_La prediction (**15**). Based on superficial gas velocity (u_g) and power input per unit volume (P/V), the model effectively predicts k_La values across a breadth of power inputs and gas velocities. The general form of that correlation is (**16**):

Equation 5: $$k_La = 0.022(P/V)^{0.7} \times u_g^{0.5}$$

Equation 5 can be rearranged as shown below to solve for the superficial gas velocity. Then, Equation 7 enables calculation of the required gas flow rate (in m^3/s).

Equation 6: $$u_g = \left(\frac{k_La}{0.022(P/V)^{0.7}}\right)^{1/0.5}$$

Equation 7: $$Q_g = u_g \times A_{S,T}$$

$A_{S,T}$ represents the cross-section area of a tank (in m^2). That empirical correlation allows for practical estimation of k_La by integrating operational parameters. Researchers and process engineers can predict how changes in gas flow and power input influence oxygen-transfer rates. Doing so is essential for designing STRs for cell-culture processes when k_La is unknown. P/V values significantly influence oxygen-transfer efficiency and overall process performance. Recommended values differ with scale, ranging 15 to 50 W/m^3 (**17**).

Sparger Length, Hole Diameter, Gas Entrance Velocity, and Pressure Drop: During design of drilled-hole spargers, equipment engineers must make precise calculations for sparger pipe diameter and for hole diameter, number, and spacing to optimize gas dispersion and mass-transfer efficiency.

Once equipment engineers have determined the total required gas-flow rate, they can calculate sparger-hole diameter (d_h) values to suit specific process requirements. According to Sandadi et al., drilled-hole tube spargers commonly have hole diameters between 0.5 and 1 mm (**18**). Small diameters within that range are particularly effective for generating fine bubbles, which are ideal for STRs with volumes <500 L. For example, HyPerforma single-use

bioreactors (Thermo Fisher Scientific) feature d_h values of 0.2 mm for systems of 50 to 100 L, 0.23 mm for 250-L reactors, 0.4 mm for 500-L vessels, and 0.58 mm for 2000-L systems (**19**). Sartorius BioStat single-use bioreactors feature a standard hole size of 0.8 mm for systems of 50–2000 L, with increasing numbers of holes to accommodate larger scales (**6**). Cytiva XDR single-use STRs typically feature sparger-hole diameters of 0.5 to 1.0 mm for systems up to 2000 L (**20**). Yunos et al. have observed that d_h values between 0.5 and 1.25 mm can generate bubbles of 5–7 mm in diameter depending on gas velocities (**21**). Such parameters are optimal for maintaining cell-culture health and performance.

For large-scale reactors, d_h values must increase to accommodate high gas-flow rates and ensure effective gas–liquid interactions. Khan has reported use of stainless-steel STRs with sparger-hole sizers of 4.0 mm for 20,000-L systems and 1.5 mm for 1000-L and 4000-L vessels (**3**). Similarly, Bruninghaus et al. (**22**) and Li et al. (**23**) have documented d_h values of 1.0 mm and 1.6 mm, respectively, for stainless-steel bioreactors with capacities of up to 20,000 L. Such systems are designed to support high gas-flow rates with a gas-entrance velocity (G_{EV}) of up to 65 m/s.

Selecting an appropriate d_h size is critical for balancing gas flow, mass-transfer efficiency, and shear stress, especially for sensitive cell cultures. Bioreactor design should begin with the smallest diameter suitable for a system's scale, allowing for subsequent adjustments to meet specific requirements for gas-entrance velocity, bubble size, spacing between bubbles, sparger-pipe length (L), pressure drops across sparger holes ($\Delta P_{Spr,hole}$), and pressure drops across the cross-sectional area of the sparger pipe (ΔP_p). Optimizing such features ensures that a system will operate at peak efficiency.

Amer et al. have found that a ring sparger with a diameter (L) of 0.8× the impeller diameter (d_i) shows improved gas hold-up and mass-transfer efficiency across a range of impeller speeds (**24**).

In a sparger, gas naturally tends to take the path of least resistance. If a pressure drop across the sparger holes is too low, then gas might flow predominantly through one or a few holes, leading to uneven gas distribution throughout a bioreactor. The pressure drop across the sparger hole can be modeled using the Darcy–Weisbach equation (**25**):

Equation 8: $$\Delta P_{Spr,hole} = \frac{\rho_g \times {G_{EV}}^2}{2 \times {C_d}^2}$$

Therein, C_d is the discharge coefficient, with 0.65 being a good approximation (**26**). Benz (**4**) and related studies (**24, 27**) have reported that, to prevent uneven gas flow across sparger holes, the sparger should be kept level, and the pressure drop across the sparger hole at peak airflow should be designed to 10× the pressure drop across the gas flow through the sparger pipe.

Together, studies by Zhu et al. and Chaudhary et al. provide G_{EV} values of 30 to 60 m/s as a general range for maintaining optimal

mammalian-cell growth and productivity in STRs. Specifically, Zhu and colleagues determined that a G_{EV} exceeding 30 m/s can harm murine myeloma (NS0) cells (**28**). Meanwhile, Chaudhary's team established that a G_{EV} of 60 m/s is critical for Chinese hamster ovary (CHO) cells (**29**). However, levels above that can cause excessive shear, diminishing cell health and process efficiency.

Number of Holes, Sparger-Pipe Diameter, Hole Spacing, and Sparger Location: The required number of sparger holes (N_h) is determined by dividing the total gas flow rate (Q_g) by the flow rate per hole ($Q_{g,h}$) as shown below:

Equation 9: $$N_h = Q_g \div Q_{g,h} = \frac{Q_g}{G_{EV} \times \left(\pi(D_h{}^2) \div 4\right)}$$

Knaebel has provided a simple way (Equation 10) to characterize the relationship of sparger-hole diameter (D_h), sparger-ring diameter (D_p), and sparger-hole number (N_h) (**30**). Rearranging that equation solving for D_p yields Equation 11.

Equation 10: $$D_h \leq 0.7(D_p \div N_h{}^{1/2})$$

Equation 11: $$D_p = 1.4286 \times D_h \times N_h{}^{1/2}$$

Benz has recommended, as a rule of thumb, that the ratio of the total area of all sparger holes to the cross-sectional area of the pipe should be maintained at ≥1.0 (**4**). More precisely, the cross-sectional flow area of the sparger pipe should be at least 2× the total area of the sparger holes (**31**).

Amer et al. have identified a spacing factor (S_h) of 3.5–4.5× the hole diameter as effective for optimizing gas distribution and pressure drops in microbial fermentors (**24**). Both Karimi et al. (**27**) and Hamood-Ur-Rehman et al. (**32**) recommend S_h values between 3 and 5 to accommodate different reactor scales and operational parameters. Karimi et al. specifically demonstrate that an S_h of 4 achieves optimal gas hold-up and oxygen-transfer efficiency in aerobic fermentation systems (**27**). Those insights suggest that a spacing factor of 3.5 to 4.0 should provide a practical range for most applications, with possibility for adjustment based on reactor scale, liquid properties, and process conditions to enhance mass transfer and operational performance.

To ensure uniform distribution of gas flow across all holes along the length of a sparger, the $\Delta P_{Spr,hole}$ value should be 10× the pressure drop across sparger length ($\Delta P_{Spr,lgt}$). The latter parameter is given by Equation 12. Therein, f is the fanning friction factor, L is the sparger length, ρ_g is the gas density, and ϑ is the cross-velocity of gas across the internal diameter of a sparger pipe (**33**).

Equation 12: $$\Delta P_p = f \times \frac{L}{D_p} \times \frac{\rho_g \times \vartheta^2}{2}$$

A sparger typically is mounted near the bottom of a bioreactor, often positioned within 0.1–0.4× the position of the lowest impeller. Such placement helps in maximizing gas distribution throughout a reactor while preventing direct interference with an impeller's flow pattern (**3, 7**).

Assess the Maximum Process Flow Rate To Account for Impeller Flooding: *Impeller flooding* arises when an impeller becomes excessively submerged, disrupting its ability to mix and aerate a culture medium. That phenomenon often stems from very high gas rates or insufficient impeller speeds, which can generate buoyancy forces that overwhelm an agitator's pumping action. Warmoeskerken and Smith have provided an empirical correlation to predict the flooding point, as shown below (**34**):

Equation 13: $$N_a > \left(30 \times N_{Fr} \times \left(\frac{d_i}{D_T}\right)^{3.5}\right)$$

Therein, the STR aeration number (N_a) is a dimensionless parameter that describes the ratio of gas flow rate to impeller speed and diameter, as calculated here (**4, 7, 11**):

Equation 14: $$N_a = Q_g \div (N \times d_i^3)$$

Froude's number (*Fr*) is a dimensionless parameter used in bioreactor design to characterize the balance between inertial forces and gravitational forces in a fluid system, particularly in STRs. It helps in understanding flow behavior, especially when scaling up bioreactors and assessing the impact of impeller speed on fluid flow (Equation 15) (**4, 7, 11**).

Equation 15: $$N_{Fr} = (N_i^2 \times D_i) \div g$$

Assess Bubble Size and CO_2 Removal Efficiency: The Sauter mean bubble diameter (d_b) can be approximated using the empirical relationship modeled below (**35**):

Equation 16: $$d_b = 1.17 \times G_{EV}^{0.4} \times d_h^{0.8} \times g^{-0.2}$$

Microbubbles (with diameters of <0.1 mm) are known to diminish cell health and productivity. In such cases, bubble movement is dominated by liquid surface tension, which reduces bubble-rise velocity and extends bubble residency times within a bioreactor. The result is inefficient CO_2 removal from a cell culture (**14**). Although small bubbles provide higher mass-transfer areas than large bubbles do, they exhibit slower rising velocities and reduced CO_2 driving forces. Muralidharan et al. demonstrated theoretically that a bubble size of 10 mm is optimal for balancing oxygen transfer and CO_2 removal (**14**). Under low gas-flow rates and agitation levels that are typical for animal-cell culture, the sizes of bubbles generated at the sparger are likely to be consistent with those elsewhere in the bioreactor (**14**). A bubble size of 10 mm

also aligns with previously recommended bubble sizes: Varley and Birch (**35**) suggest 5–6 mm, and Khan proposes 10–20 mm (**3**).

As bubbles are introduced into STRs, shear can be assessed at three stages. The first point is at the surface of the sparger holes. There, shear is calculated in terms of G_{EV} (see "Supplemental Equations 1").

The second measurement possibility occurs as bubbles rise through the bioreactor liquid height. Shear levels can be determined through calculation of the *bubble-wake eddy length*: As bubbles rise, they carry circulating fluid behind them, resulting in microeddies. A bubble-wake eddy length that is less than or equal to the size of the cultured cells will harm them. Hence, good design practice for most mammalian-cell cultures calls for eddy lengths of >20 µm to prevent negative effects on cell growth.

The third measurement stage occurs when bubbles burst at the gas–liquid interface. As a bubble rises, cells become trapped in the film around it. On reaching the gas–liquid interface, a cavity forms on the bubble surface. The cavity soon collapses, forming a liquid jet as the bubble bursts and disappears. Cells carried in the bubble-film volume will die from shear when the jet forms and the bubble disintegrates. Bubble-burst shear is assessed by determining the burst energy-dissipation rate (EDR), calculated as a function of bubble diameter.

Muralidharan et al. developed a predictive model to evaluate shear stress associated with bubble bursting (**10**). That model leverages a nonlinear exponential approach, derived from data provided by Boulton-Stone and Blake (**37**). The model is designed to offer a robust framework for assessing shear stress in STR systems.

EDRs of around 10^4 W/m^3 are typically sublethal for most cell-culture processes. Thus, associated shear levels generally do not damage cells significantly (**38**). In summary, considering the balance between shear and CO_2 stripping, sparger designs should aim to generate bubble sizes of 5–20 mm.

The above approach to drilled-hole sparger design assumes that the maximum G_{EV} does not exceed 60 m/s, ensuring that shear from bubble generation at the sparger-hole surface remains negligible. As demonstrated in Figure 3, the EDR from bubbles bursting at the liquid surface comes to 10^3 W/m^3, which is well

Supplemental Equations 1: Bubble-rise and bubble-burst shear assessment (**19, 24, 36**)

Shear When a Bubble Rises Through the Bioreactor Liquid Height — Bubble-Rise Eddy Length (36)

Bubble area (m^2): $A_b = \frac{\pi d_b^2}{4}$

Bubble velocity (m/s): $\theta_b = \left(\frac{2\sigma}{d_b \rho} + \frac{0.5 d_b}{g}\right)^{1/2}$

Drag force from bubble (kg·m/s^{-2}): $F_b = (C_d \times \theta_b^2 \times A_b \times \rho) \div 2$

Bubble EDR (W/m^3 or kg·m^2/s^{-3}): $F_b \times \theta_b$

Specific EDR (W/kg): $\varepsilon_b = 0.8 \times (EDR) \div \left(\frac{\pi d_b^3}{6}\, m^3 \times 1000 \frac{kg}{m^3}\right)$

Bubble Eddy Length: $\eta_b = 10^6 \times \frac{\nu^3}{\varepsilon_b}$

Shear When a Bubble Bursts at the Gas–Liquid Interface — Bubble-Burst Eddy Length

$EDR_{burst} = e^{[-194.43 \times (\log(d_b))^3] - [217.02 \times (\log(d_b))^2] - [129.07 \times (\log(d_b))] - 19.599}$

Here, bubble diameter (d_b) is calculated in centimeters.

A_b = bubble surface area, C_d = drag coefficient for rising bubbles, assumed to be 2.6 (dimensionless) (**19, 24**), d_b = bubble diameter, **EDR** = energy-dissipation rate, EDR_{burst} = bubble-burst energy-dissipation rate, F_b = bubble drag force, g = gravitational acceleration, ε_b = dissipated kinetic energy per unit mass, η_b = bubble eddy length, θ_b = bubble velocity, ν = fluid kinematic viscosity (9.8 × 10^{-7} m^2/s), ρ = liquid density (1015 kg/m^3), σ = liquid surface tension (0.65 N/m)

below levels that would compromise cell-culture performance. That finding is consistent for sparger-hole sizes of 0.25 to 3.25 mm, even under the maximum assumed G_{EV} of 60 m/s.

However, Figure 3 highlights a limitation in bubble-rise eddy length when sparger-hole diameters reach 1.75 mm. At that diameter, eddy lengths exceed 40 µm. Although maintaining an EDR above 20 µm is considered to be safe for cell-culture operations, best practices for sparger design account for potential bubble coalescence under STR conditions. The generally accepted engineering principle is to use a safety factor of 2 to address uncertainties and ensure reliability under worst cases (**39**). Such a conservative approach should account for variability in bubble dynamics and turbulence, which could generate larger-than-expected bubbles or cause EDR deviations during operation. Thus, it is advisable to design sparger-hole sizes to achieve an eddy length greater than 2 × 20 µm = 40 µm to ensure robust and consistent performance.

Figure 3: Sparger-hole size (D_h) against bubble-rise microeddy length and bubble-burst energy dissipation rate (EDR)

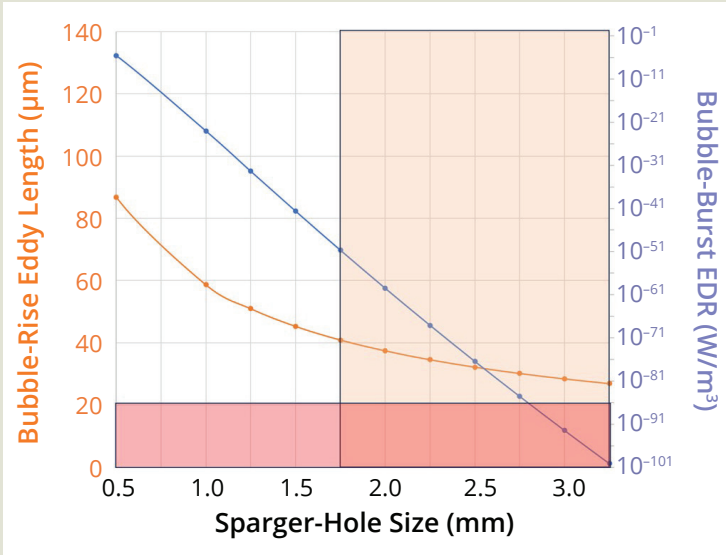

Supplemental Equations 2: Calculation of total mass-transfer surface area from bubbles generated at a sparger hole (per unit of gas-flow rate)

Volume of a Single Bubble: $V_b = \pi \frac{d_b^3}{6}$

Number of Bubbles Generated (per unit time): $N_b = Q_g \div V_b$

Area of a Single Bubble: $A_b = \pi d_b^2$

Total Mass-Transfer Area (per unit gas flow rate): $A_{TNB} = A_b \times N_b$

A_b = bubble area, A_{TNB} = total mass-transfer surface area, d_b = bubble diameter, N_b = number of bubbles generated, Q_g = gas flow rate

Optimize Sparger-Hole Design for Efficient Mass Transfer and Shear Control: As discussed above, researchers have reported sparger-hole sizes of 0.5 to 4.0 mm for large-volume STRs, depending on the scale of operation. Configurations differ significantly across bioreactor designs and manufacturers. Therefore, equipment engineers must understand process requirements and priorities from an end-user perspective, both to ensure efficient cell-culture applications and to harmonize methodologies for sparger design.

Sparger design must account for shear potential from bubble bursting (e.g., by establishing an EDR of <10^3 W/m³), gas entrance velocity (G_{EV} < 60 m/s), and target bubble size (5–10 mm). The optimal sparger-hole size should maximize the total mass-transfer surface area of the bubbles generated per unit of gas flow rate while adhering to shear-related parameters and bubble-size requirements. The "Supplemental Equations 2" box details calculations for the total mass-transfer surface area generated per unit gas flow rate based on different sparger-hole sizes.

To illustrate the concepts discussed above, we performed calculations for sparger-hole size using a gas flow rate of 0.05 vvm

and a G_{EV} value of 60 m/s. Figure 4 plots those values against calculations for bubble size and total mass-transfer surface area generated per unit gas flow rate for three bioreactor scales. Based on established bubble-size constraints (5.0–20 mm, to ensure effective CO_2 removal) and a sparger-hole size of 1.75 mm at a G_{EV} of 60 m/s (to maintain the bubble-rise microeddy length below 40 µm), we determined optimal sparger configurations, shown in the white region in Figure 4. The "Typical Bioreactor Settings" box summarizes corresponding ranges for those configurations across bioreactor scales of 10,000–20,000 L.

Figure 4: Optimization of sparger-hole size (D_h) for bioreactors of different scales when accounting for bubble diameter and the total mass-transfer area from bubbles generated a sparger hole (area per unit of gas-flow rate)

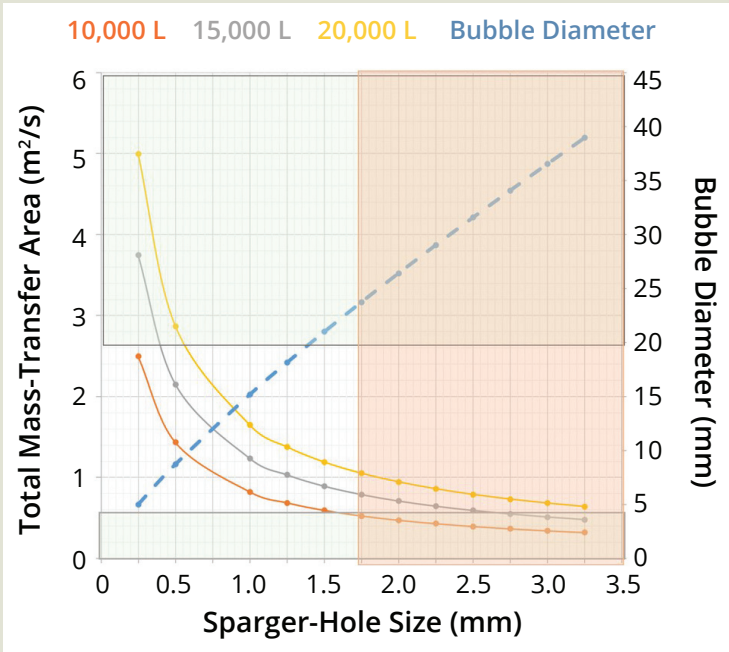

Gas Filter Area Sizing

Bioreactor design requires meticulous consideration of hydrophobic-filter sizing for both sparger and exhaust systems to ensure effective gas management and sterile conditions. For both sparger and exhaust or vent applications, hydrophobic filters (typically with a pore size of 0.2 µm) are crucial to preventing contamination by retaining particulates and microorganisms before they can enter a bioreactor. The filter area must be sufficient to accommodate the desired gas-flow rate. Filters used in fermentation processes are required to meet high microbial-retention standards and provide high flow rates with relatively low pressure drops (1–5 psi) (**40**). Vendors of 0.2-µm hydrophobic filters often provide data sheets with graphs plotting pressure against gas flow rate per filter area. From those materials, users can select the required filter area based on the gas-flow rate needed to ensure that pressure drops remain between 1 and 5 psi.

Mass-Flow Controller Selection for Typical Bioreactor Gas-Flow Rates

Bioreactor design also involves selection of mass-flow controllers (MFCs). Selection is based on different gas-flow rates. The bottom of the "Typical Bioreactor Settings" box summarizes cell-culture gas flow rates for spargers and headspace volumes (**1**).

Improving Upstream Production

STR design plays a pivotal role in optimizing cell growth and maximizing productivity during biopharmaceutical production. Our review has highlighted the importance of critical design elements, such as vessel aspect ratio, impeller selection, and sparger configuration, with particular emphasis on mitigating shear stress and improving gas–liquid interactions. Addressing potential problems such as impeller flooding and ensuring efficient mixing

Typical Bioreactor Settings

Recommended Sparger Configurations (0.05 volumes of gas per volume of liquid per minute (vvm), 60 m/s, with no detrimental impact to cell culture):

10,000 L: 2831 × 0.25 mm, 708 × 0.50 mm, 177 × 1.00 mm, 113 × 1.25 mm, 79 × 1.50 mm

15,000 L: 1026 × 0.5 mm, 265 × 1.00 mm, 170 × 1.25 mm, 118 × 1.50 mm, 87 × 1.75 mm

20,000 L: 354 × 1.0 mm, 226 × 1.25 mm, 157 × 1.50 mm, 116 × 1.75 mm

Typical Gas-Flow Rates for Mammalian-Cell Cultures (**1**):

Sparger Air: 0.001–0.05 vvm

Sparger O_2: 0.001–0.05 vvm

Sparger CO_2: 0.001–0.01 vvm

Sparger N_2: 0.001–0.01 vvm

Headspace Air: 0.01–0.1 vvm

Headspace N_2: 0.01–0.1 vvm

Back to Contents

are vital for maintaining desired cell-culture environments. Furthermore, advanced designs for drilled-hole spargers and appropriate sizing of vent filters have been shown to enhance bioreactor performance significantly. By incorporating insights from published studies into bioreactor design and operation, biomanufacturers can achieve high protein yields, improve product quality, and enhance process efficiency. Ultimately, we want our review to serve as a useful guide for industry professionals aiming to refine STR technology and optimize cell-culture applications, contributing to the ongoing advancement of bioprocess technologies.

References

1 Ernest L. *Fermentor/Bioreactor Design* (presentation). Bioprocess Equipment Seminar. B. Braun Biotech Inc.: Atlanta, GA, 1 October 2001.

2 *Mixing 101: Baffled by Baffles? How Baffle Configuration Can Optimize Industrial Mixing*. Dynamix Inc., 19 October 2012; https://dynamixinc.com/baffled-by-baffles.

3 Khan M. *Patent App. No. 2011/0312087 A1: Bioreactor for the Cultivation of Mammalian Cells*. US Patent and Trademark Office: Washington, DC, 22 December 2011; https://patentimages.storage.googleapis.com/7d/5f/26/2366cacbcbe985/US20110312087A1.pdf.

4 Benz GT. *Agitator Design for Gas–Liquid Fermenters and Bioreactors*. Wiley/American Institute of Chemical Engineers, Inc.: Hoboken, NJ, 13 April 2021.

5 Mirro R, Voll K. Which Impeller Is Right for Your Cell Line? *BioProcess Int.* 1(7) 2009: 52–57; https://www.bioprocessintl.com/cell-line-development/which-impeller-is-right-for-your-cell-line-.

6 De Wilde D, et al. Superior Scalability of Single-Use Bioreactors. *BioProcess Int.* 12(8s) 2014: 14–19; https://www.bioprocessintl.com/single-use/superior-scalability-of-single-use-bioreactors.

7 Doran PM. *Bioprocess Engineering Principles*, Second Edition. Academic Press: Cambridge, MA, 2013.

8 Lara AR, et al. Living with Heterogeneities in Bioreactors: Understanding the Effects of Environmental Gradients on Cells. *Mol. Biotechnol.* 34(3) 2006: 355–381; https://doi.org/10.1385/MB:34:3:355.

9 Muralidharan N, Bolduc E, Davis M. Strategies Used in Manufacturing Processes To Drive and Control Mammalian Cells To Undergo a Lactate Metabolic Shift. *Pharm. Bioprocessing* 12(2) 2024: 152–157; https://www.openaccessjournals.com/articles/strategies-used-in-manufacturing-processes-to-drive-and-control-mammalian-cells-to-undergo-a-lactate-metabolic-shift.pdf.

10 Muralidharan N, Bolduc E, Davis M. Characterizing Oxygen Mass Transfer and Shear During Cell Culture: Calculating the Maximum Cell Density Supported by a 20,000-Liter Stirred-Tank Bioreactor. *BioProcess Int.* 22(1–2) 2024: 38–46; https://www.bioprocessintl.com/bioreactors/characterizing-oxygen-mass-transfer-and-shear-during-cell-culture-calculating-the-maximum-cell-density-supported-by-a-20-000-liter-stirred-tank-bioreactor.

11 Shuler ML, Kargi F, DeLisa MP. *Bioprocess Engineering: Basic Concepts*, Third Edition. Pearson: London, UK, 2017.

12 Bauer I, et al. *Recommendations for Process Engineering Characterisation of Single-Use Bioreactors and Mixing Systems by Using Experimental Methods*, Second Edition. DECHEMA: Frankfurt, Germany, 2020; https://dechema.de/dechema_media/Downloads/Positionspapiere/Single_Use_BioReactors_2020-p-20006899.pdf.

Back to Contents

13 Bowers JS. Sparger and Surface Gas Transfer for Cell Culture Bioreactors. *Proc. AIChE Annu. Meet.* November 2008; https://skoge.folk.ntnu.no/prost/proceedings/aiche-2008/data/papers/P118781.pdf.

14 Muralidharan N, et al. CO_2 Control Strategy for Large-Scale Cell Culture Bioreactor Operation. *Adv. Biosci. Bioeng.* 12(1) 2024: 1–13; https://doi.org/10.11648/abb.20241201.11.

15 van 't Riet, K. Review of Measuring Methods and Results in Nonviscous Gas–Liquid Mass Transfer in Stirred Vessels. *Ind. Eng. Chem. Process Des. Dev.* 18(3) 1979: 357–364; https://doi.org/10.1021/i260071a001.

16 Vanags J, Suleiko A. Oxygen Mass Transfer Coefficient Application in Characterisation of Bioreactors and Fermentation Processes. *Latvian J. Phys. Tech. Sci.* 59(5) 2022: 21–32; https://doi.org/10.2478/lpts-2022-0038.

17 Muralidharan N. Shear-Proof Design Space: Scaling Stirred-Tank Bioreactors for Cell Culture Processes. *BioProcess Int.* 21(1–2) 2023: 35–37, 45; https://www.bioprocessintl.com/bioreactors/shear-proof-design-space-scaling-stirred-tank-bioreactors-for-cell-culture-processes.

18 Sandadi S, et al. A Comprehensive Comparison of Mixing, Mass Transfer, Chinese Hamster Ovary Cell Growth, and Antibody Production Using Rushton Turbine and Marine Impellers. *Bioprocess Biosys. Eng.* 34(7) 2011: 819–832; https://doi.org/10.1007/s00449-011-0532-0.

19 *Data Sheet 091: HyPerforma Single-Use Bioreactor — Bioprocess Containers with Drilled-Hole Sparger.* Thermo Fisher Scientific: Waltham, MA, 2016; https://assets.thermofisher.com/TFS-Assets/LSG/brochures/PG1520-PJ8211-C0020203-SUB-BPC-wDrilled-Hole-Sparger-Datasheet-Americas-FLR.pdf.

20 Tuohey C, et al. *Patent No. 9,969,965 B2: Linearly Scalable Single-Use Bioreactor System*. US Patent and Trademark Office: Washington, DC, 15 May 2018; https://patentimages.storage.googleapis.com/dd/9e/89/f902f73cff8c7a/US9969965.pdf.

21 Yunos MASM, et al. Investigations of Bubble Size, Gas Hold-Up, and Bubble Rise Velocity in Quadrilateral Bubble Column Using High-Speed Camera. *Am. J. Eng. Technol. Soc.* 4(1) 2017: 5–15; http://www.openscienceonline.com/journal/archive2?journalId=737&paperId=3685.

22 Bruninghaus M, et al. *Patent No. AU 2021245116 B: Seed Train Processes and Uses Thereof.* IP Australia: Canberra, Australia, 28 October 2021; https://patentimages.storage.googleapis.com/34/be/a3/76a2106e720626/AU2021245116B2.pdf.

23 Li F, et al. *Patent No. 10,023,831 B2: Gas Delivery Devices and Associated Systems and Methods*. US Patent and Trademark Office: Washington, DC, 17 July 2018; https://patentimages.storage.googleapis.com/0a/0b/36/d503c90829b975/US10023831.pdf.

24 Amer MA, Feng Y, Ramsey JD. Using CFD Simulations and Statistical Analysis To Correlate Oxygen Mass Transfer Coefficient to Both Geometrical Parameters and Operating Conditions in a Stirred-Tank Bioreactor. *Biotechnol. Prog.* 35(3) 2019: e2785; https://doi.org/10.1002/btpr.2785.

25 Backhurst JR, Harker JH, Richardson JF. *Chemical Engineering*, Volume 1: Fluid Flow, Heat Transfer and Mass Transfer, Sixth Edition. Butterworth-Heinemann: London, UK, 1999.

26 *Technical Paper 410: Flow of Fluids Through Valves, Fittings, and Pipe*. Crane ChemPharma and Engineering Corp.: Suffolk, UK, 2022.

27 Karimi K, et al. Oxygen Mass Transfer in a Stirred Tank Bioreactor Using Different Impeller Configurations for Environmental Purposes. *Iranian J. Environ. Health Sci. Eng.* 10(1) 2013: 6; https://doi.org/10.1186/1735-2746-10-6.

Further Reading on Bioreactor Scale-Up

For more information about bioreactor design and cell-culture operation, be sure to read Muhammad Arshad Chaudhry's continuing series, titled "Lessons in Bioreactor Scale-Up." Below are the installments currently available on the BPI website.

Part 1: Exploring Introductory Principles (January–February 2024); https://www.bioprocessintl.com/bioreactors/lessons-in-bioreactor-scale-up-part-1-mdash-exploring-introductory-principles.

Part 2: A Refresher on Fluid Flow and Mixing (June 2024); https://www.bioprocessintl.com/bioreactors/lessons-in-bioreactor-scale-up-part-2-a-refresher-on-fluid-flow-and-mixing.

Part 3: Experimental Determination and Application of Oxygen Mass-Transfer Rate, Mass-Transfer Coefficient, and Oxygen-Uptake Rate (September 2024); https://www.bioprocessintl.com/bioreactors/lessons-in-bioreactor-scale-up-part-3-experimental-determination-and-application-of-oxygen-mass--transfer-rate-mass-transfer-coefficient-and-oxygen-uptake-rate.

Part 4: Physiochemical Factors Affecting Oxygen Transfer and the Volumetric Mass-Transfer Coefficient in Stirred Tanks (October 2024); https://www.bioprocessintl.com/bioreactors/lessons-in-bioreactor-s-scale-up-part-4-physiochemical-factors-affecting-oxygen-transfer-and-the-volumetric-mass-transfer-coefficient-in-stirred-tanks.

Part 5: Theoretical and Empirical Correlations for Predicting the Mass-Transfer Coefficient in Stirred-Tank Bioreactors (January–February 2025); https://www.bioprocessintl.com/bioreactors/lessons-in-bioreactor-scale-up-part-5-theoretical-and-empirical-correlations-for-predicting-the-mass-transfer-coefficient-in-stirred-tank-bioreactors.

28 Zhu Y, et al. NSO Cell Damage by High Gas Velocity Sparging in Protein-Free and Cholesterol-Free Cultures. *Biotechnol. Bioeng.* 101(4) 2008: 751–760; https://doi.org/10.1002/bit.21950.

29 Chaudhary G, et al. Understanding the Effect of High Gas Entrance Velocity on Chinese Hamster Ovary (CHO) Cell Culture Performance and Its Implications on Bioreactor Scale-Up and Sparger Design. *Biotechnol. Bioeng.* 117(6) 2020: 1684–1695; https://doi.org/10.1002/bit.27314.

30 Knaebel KS. Simplified Sparger Design. *Chem. Eng.* 88(5) 1981: 116–118.

31 *Guidelines for Pressure Relief and Effluent Handling Systems*, Second Edition. Wiley/Center for Chemical Process Safety: Hoboken, NJ, 2017.

32 Hamood-ur-Rehman M, Ein-Mozaffari F, Dahman Y. Dynamic and Local Gas Holdup Studies in External Loop Recirculating Airlift Reactor with Two Rolls of Fiberglass Packing Using Electrical Resistance Tomography. *J. Chem. Technol. Biotechnol.* 88(5) 2013: 887–896; https://doi.org/10.1002/jctb.3917.

33 Perry RH, Green DW, Maloney JO. *Perry's Chemical Engineers' Handbook*, Eighth Edition. McGraw-Hill: New York, NY, 2008.

34 Warmoeskerken MMCG, Smith JM. Flooding of Disc Turbines in Gas–Liquid Dispersions: A New Description of the Phenomenon. *Chem. Eng. Sci.* 40(11) 1985: 2063–2071; https://doi.org/10.1016/0009-2509(85)87023-8.

35 Varley J, Birch J. Reactor Design for Large Scale Suspension Animal Cell Culture. *Cytotechnology* 29(3) 1999: 177–205; https://doi.org/10.1023/A:1008008021481.

36 Chisti Y. Animal-Cell Damage in Sparged Bioreactors. *Trends Biotechnol.* 18(10) 2000: 420–432; https://doi.org/10.1016/s0167-7799(00)01474-8.

37 Boulton-Stone JM, Blake JR. Gas Bubbles Bursting at a Free Surface. *J. Fluid Mech.* 254, 1993: 437–466; https://doi.org/10.1017/S0022112093002216.

38 Hu W, Berdugo C, Chalmers JJ. The Potential of Hydrodynamic Damage to Animal Cells of Industrial Relevance: Current Understanding. *Cytotechnology* 63(5) 2011: 445–460; https://doi.org/10.1007/s10616-011-9368-3.

39 Budynas RG, Nisbett JK. *Shigley's Mechanical Engineering Design*, 11th Edition. McGraw-Hill Education: New York, NY, 2020.

40 TR40. *Sterilizing Filtration of Gases*, Second Edition. Parenteral Drug Association: Bethesda, MD, 2005.

About the Authors

Tyler Younger, ***Grace Chan***, ***Shandilyn Ball***, *and* ***Emma Bolduc*** *are manufacturing science and technology (MSAT) engineers;* ***Mark Davis*** *is director of MSAT; and corresponding author and BPI editorial advisor* ***NaveenGanesh Muralidharan*** *(nmural@agcbio.com) is senior manager of the MSAT team, all at AGC Biologics, 5550 Airport Boulevard, Boulder, CO 80301; https://www.agcbio.com.*

Back to Contents

Accelerating Bioreactor Design with Computational Fluid Dynamics Modeling

A Deep Dive into the Development Processes Underlying a Next-Generation Bioreactor

Ken Clapp

Industry demand for mammalian cell cultures of increasingly high productivity and robustness has driven the need for high-performing, scalable, and modality-agnostic bioreactors. Such requirements affect process developers and bioreactor manufacturers alike: Efficient design and predictable scalability are key to reaching program milestones on time. Understanding nonmeasurable parameters (such as shear rate and turbulence) and demonstrating scalability are vital to meeting performance criteria.

Computational fluid dynamics (CFD) modeling can reduce experimental requirements in bioreactor design by simulating bioreactor geometry, fluid flow, and component design and positioning. Herein, we discuss how we used CFD modeling to accelerate agitator and sparger design for the next-generation Xcellerex X-platform bioreactor and to predict shear stress and concentration gradients.

Figure 1: Outline of phases during codevelopment of our bioreactor product and computational fluid dynamics (CFD) model; G-L = gas–liquid model, L-L = liquid–liquid model

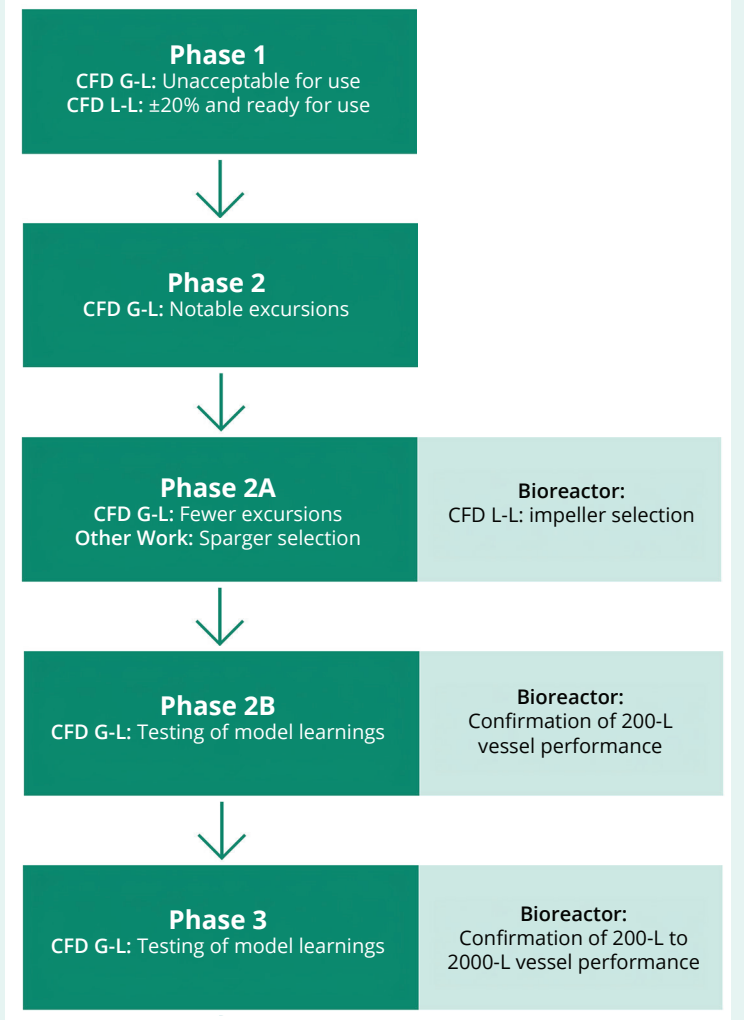

CFD-Model and Bioreactor Development Stages

We leaned on agile ways of working to develop our CFD model so that it would capture current and future bioreactor geometries and behaviors. Designing the tool and bioreactor simultaneously enabled us to condense product-development time and confirm final-product performance.

We verified the tool at different time points and used it "at risk" for key bioreactor-geometry verification work. To reduce risk, we developed the CFD model in parallel with continued "wet" testing

Back to Contents

Figure 2: Computational fluid dynamics (CFD) model from phase 1 describing liquid–liquid mixing; (LEFT) the confirmed 200-L tank geometry; (RIGHT) predicted and experimental mixing-time values (T95 = time to reach 95% homogeneity)

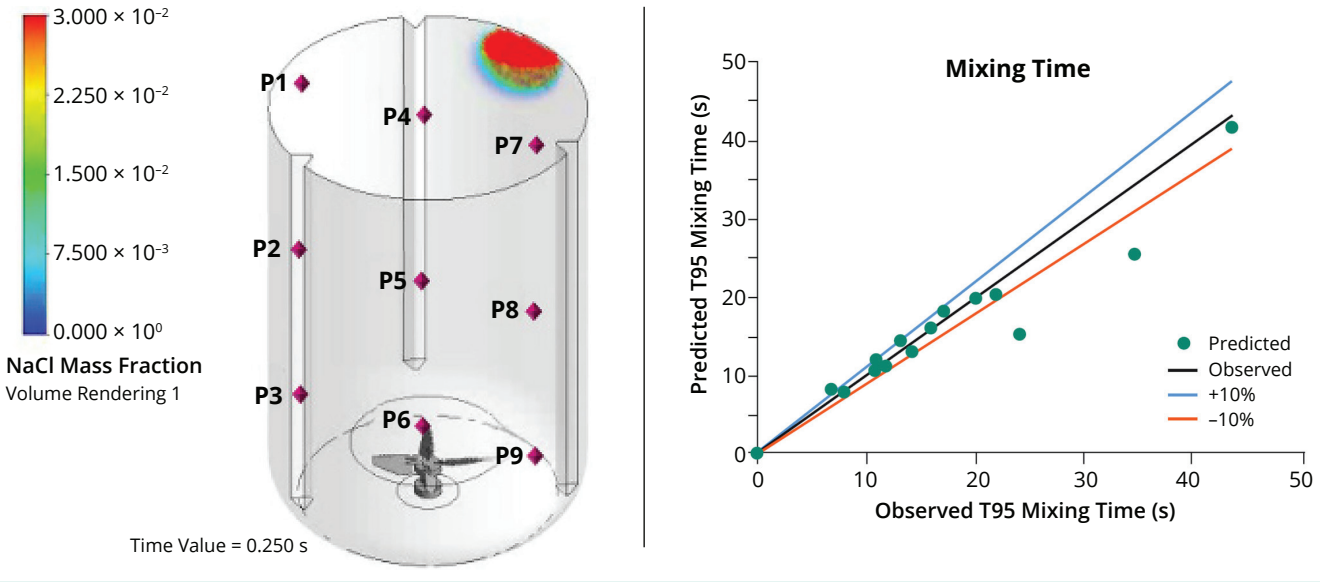

of early component designs (e.g., impeller types, sparge options, and baffle configurations), optimizing performance yet still reducing the need for further testing.

After tuning the tool for liquid–liquid (L-L) performance, we used it for early screening of interim designs. Later, once a gas–liquid (G-L) CFD model was available, outputs for shear and turbulence were used to confirm that the final bioreactor design operated within targeted performance behavior (Figure 1, previous page).

Phase 1: Confirm 200-L Tank Geometry and CFD Liquid–Liquid Model

We determined model conditions for the bioreactor tank geometry and established preliminary fluid assumptions. We used both the current Xcellerex XDR bioreactor geometry and a new bioreactor design to ensure the model's suitability for our project. Our goals at this stage were to establish and test the first pass of the single-phase CFD L-L model, to establish and test the first pass of the two-phase CFD G-L model, and to consider new target geometries and customer applications (e.g., viscosity, bubble size, agitation, and gas flow rate).

We tested an early G-L model against experimental results to identify gaps in the model's predictions. To verify the model's performance, we used oxygen mass-transfer results that were generated empirically using a mock medium. The model presumed that Pluronic poloxamer did not influence bubble formation. Internal high-speed camera evaluations confirmed bubble sizing.

Our team used 19 design-of-experiments (DoE) conditions covering different vessel volumes, sparge rates and options, and agitation speeds to verify the early G-L model. Outputs were within ≈30% of the empirical data.

To verify the single-phase L-L model's reliability, we used empirical torque and mixing-time data (Figure 2). Meanwhile,

Back to Contents

results for the G-L model indicated the need for further tuning, which we undertook in model-development phases 2, 2A, and 2B. During phase-2 efforts, our bioreactor team used outputs from the L-L model for bioreactor product development. Phase-2 testing also allowed for occasional use of the G-L model for product-design decisions if the model performed predictably.

Phase 2: Optimize Gas–Liquid Model Accuracy

Back to Contents

In this phase, we focused on enhancing the G-L model for identifying bubble distributions and using direct bubble measurements from key sparge options. Results from tuning and testing enabled us to select the sparge porosity while the final form of the sparge elements was being settled.

We had three goals for phase-2 model development. First, we wanted to evaluate and optimize the G-L model for accurate prediction of outputs when mass transfer, shear rate, and turbulence would be used. Our second objective was to reduce process-simulation time from one to two days down to a few hours. Finally, phase-2 efforts were intended to verify the G-L model by comparison with empirical results.

When designing model inputs and assumptions for shear, turbulence, and bubble-sizing factors, we first screened the most likely and best-fitting model inputs that matched with empirical results representing application ranges for agitation and sparge-gas flow rates. Then, when necessary, we used response-surface modeling to narrow model-input selection. We used 24 condition sets to screen the behavior of key input factors. Key factors considered at this stage related to turbulence-kinetic modeling parameters.

Turbulence assumptions depend on turbulence kinetic energy (k) and energy-dissipation rate (ε). We were able to select from several factors here, including the standard k-ε, renormalization group (RNG) k-ε, realizable k-ε, Chen–Kim k-ε, optimized Chen–Kim k-ε, and Reynolds stress models. We avoided models with factors that are better suited to laminar fluid environments than to turbulent flow conditions.

Final inputs for the G-L model were verified along the full range of application performance using 10 condition sets. To confirm final model behavior, we compared predicted outputs with empirical results for torque and the volumetric oxygen mass-transfer coefficient ($k_L a$), with wet experiments performed in triplicate. Additionally, we evaluated the steadiness and transience of oxygen mass transfer behavior at different points in the culture volume and found that the predicted mass-transfer behavior reflected that observed at a single sensor.

Phase 2A: Tuning the Model for Bubble Size

Our goals in this phase were to enhance the G-L model for bubble size, to down-select sparge requirements through G-L model tuning, and to down-select an impeller design using the L-L model. We

started with an in-progress version of our next-generation bioreactor tank design and a few existing sparge designs.

We used a high-speed camera to determine an average bubble size, sampling at least 30 bubbles per image and determining the average bubble diameter across four axes of the two-dimensional images (Figure 3). With that information, we selected user inputs for bubble dispersal and coalescence to match the high-speed bubble diameter estimates. Once the bubble diameters matched, we verified model performance.

Verification consisted of experiments in sets of 10, 5, and 5 conditions for each sparge type. We compared model outputs for those conditions with empirical oxygen mass-transfer data, as well as results from the new bioreactor geometry and one of the new impeller options under consideration. The model performed within the limit of ±20%, except in low mass-transfer conditions.

Figure 3: Bubble-size analysis to assess sparge porosity options; images were taken with a high-speed camera. Values above each image are average bubble diameters.

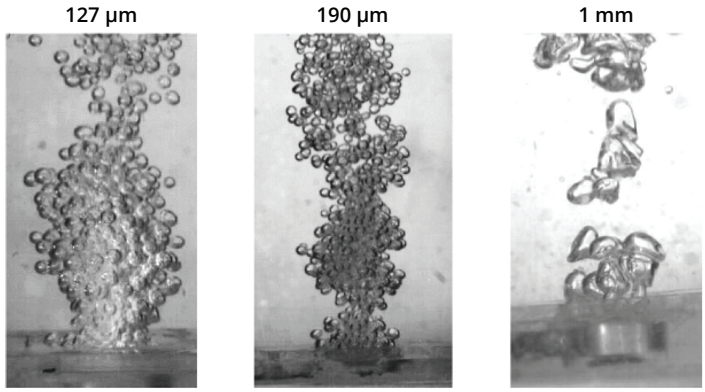

Figure 4: Model grid-size impact on gas hold-up distribution; comparing coarse, medium, and fine grid model accuracies, we chose the final grid sizing to optimize for processing time and accuracy of simulation output.

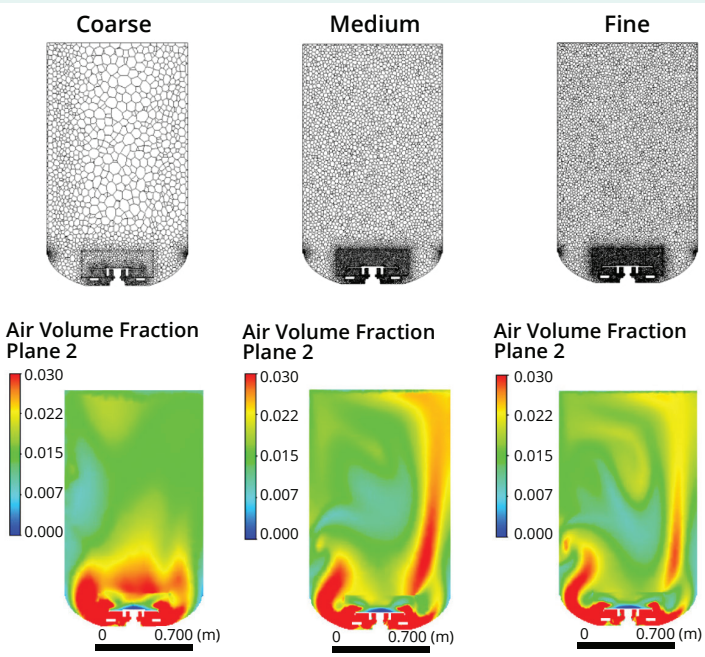

CFD Phase 2B: Near-Final Bioreactor Design

With a reliable G-L model in place, we focused on verifying it in the context of our near-final bioreactor design. Our goal was to optimize the impeller using the L-L model and then to confirm the bioreactor design and G-L model for performance in a verification experiment set. Thus, we could confirm the model and the bioreactor design simultaneously. And having determined the sparge porosity and the possible impeller form, we were able to conduct a thorough exploration of the bioreactor application range.

Testing showed consistent model behavior within ±20% of empirical results for oxygen mass transfer and torque. Results also confirmed the performance of the final 200-L bioreactor design (Figures 4 and 5).

Phase 3: Confirm Gas–Liquid Model and New Bioreactor Performance

With development of the CFD G-L model complete, we set out to confirm its behavior using a wet test of the finalized bioreactor geometry at 200-L scale. A parallel goal for bioreactor-product

Back to Contents

Figure 5: Gas–liquid computational fluid dynamics model performance after phase 2B, with predicted and observed values for (LEFT) volumetric oxygen mass transfer (k_La) and (RIGHT) torque

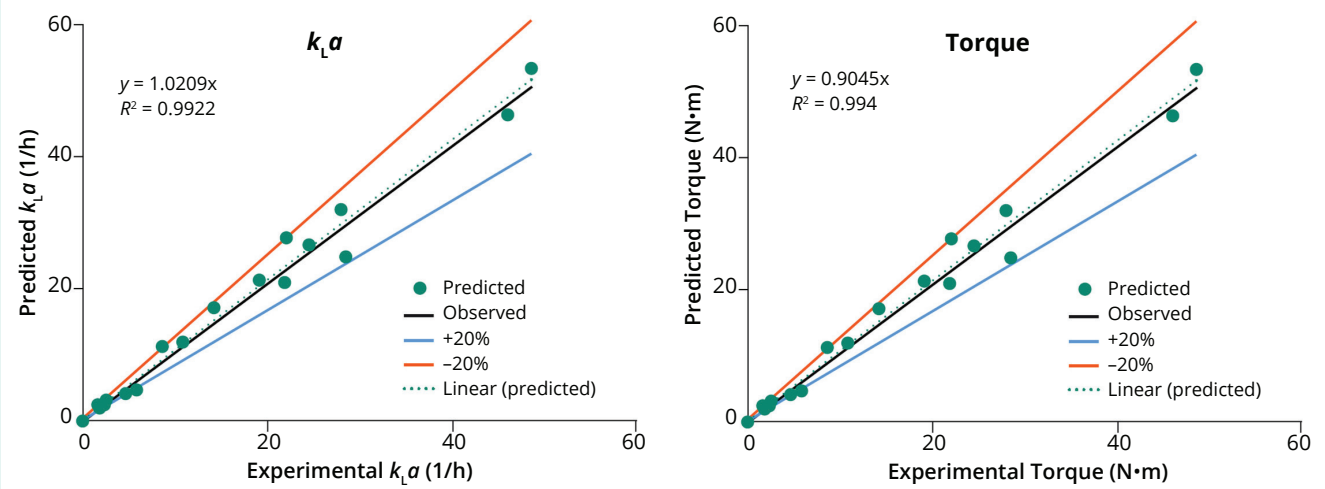

Figure 6: Computational fluid dynamics (CFD) model for Kolmogorov eddy analysis at 150 W/m^3 up-pumping and 0.2 vvm gas flow rate; turbulent eddies of <62.5 µm in diameter are represented in red. Results here are not the final performance results for the bioreactor design.

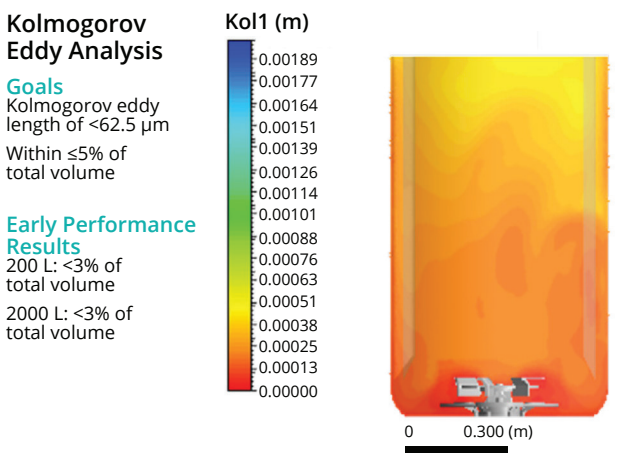

Figure 7: Computational fluid dynamics (CFD) model for shear-rate analysis, here showing velocity contours. Analysis was performed at 150 W/m^3 up-pumping and 0.2 vvm gas flow rate. Results here are not the final performance results for the bioreactor-product design.

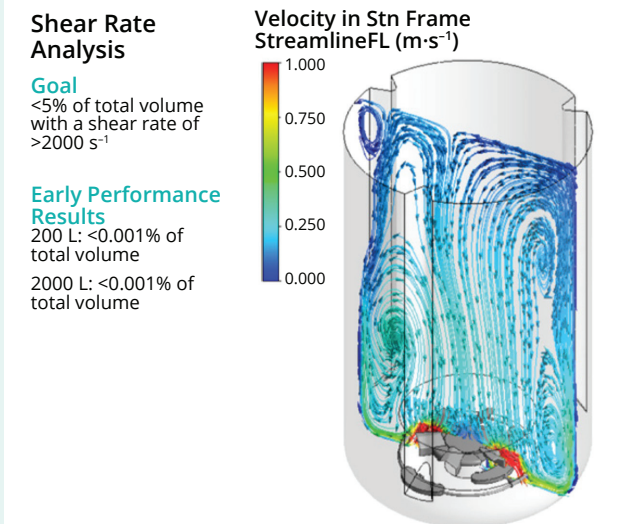

development was to confirm vessel performance for shear rate and turbulence, testing both the 200-L bioreactor and a 2000-L prototype based on geometric scaling. During this phase, all tests were based on experiments designed for each bioreactor size. We assessed both oxygen mass transfer and torque to ensure that the 200-L product was characterized fully and that we had enough data to assess the G-L model.

Results indicated that the model was within ±20% of empirical results and thus could be used to confirm the behavior of the 200-L and 2000-L bioreactors. Both formats provided the targeted performance for mixing time and mass transfer (oxygen and carbon-dioxide stripping).

Finally, we applied the G-L model to confirm design limits for shear rate and Kolmogorov eddy turbulence (Figures 6 and 7). Both

factors behaved within the requirements set for the new bioreactor design. Please note that results shown here are not the final performance values for the product design.

The Benefits of Parallel Development Activities

The CFD G-L model-development process was extremely useful for establishing the new Xcellerex X-platform bioreactor, and the process led us to a design philosophy that we can apply more generally. Now we can use a robust gas–liquid model to accelerate the development and improvement of future bioreactor designs.

That model enabled us to confirm the scalability of our new bioreactor design and to screen new features such as impeller types, sparge forms, and baffle options more efficiently than we could in previous programs. Now, all performance claims have been verified through wet testing using internal product prototypes.

The key benefits of developing a CFD model alongside a bioreactor were condensed product-development time and early access to complete characterization performance data. Compared with what we could achieve during other bioreactor-design projects, we obtained deeper quantitative insights into the predicted behavior of bioreactor design iterations in fewer performance runs.

Learn more about the Xcellerex X-platform single-use bioreactor at https://cytiva.link/hiomg.

About the Authors

Ken Clapp *is senior leader for bioreactor technology, applications, and integration at Cytiva; ken.clapp@cytiva.com.*